Polímeros
ISSN 1678-5169 (Online)

https://doi.org/10.1590/0104-1428.20230023

ORIGINAL ARTICLE

Synthesis and characterization of polyurethane and samarium(III) oxide and holmium(III) oxide composites

Lucas Repecka Alves[1], Giovanni Miraveti Carriello[1]*, Guilherme Manassés Pegoraro[1], Henrique Solowej Medeiros Lopes[1,2], Thaís de Agrella Janolla[3], Airton Natanael Coelho Dias[3], Giovanni Pimenta Mambrini[1], Maira de Lourdes Rezende[2] and Aparecido Junior de Menezes[1]

[1]Laboratório de Materiais, Programa de Pós-graduação em Ciência dos Materiais, Universidade Federal de São Carlos – UFSCar, Sorocaba, SP, Brasil

[2]Laboratório de Caracterização de Materiais Poliméricos, Faculdade de Tecnologia José Crespo Gonzales, Sorocaba, SP, Brasil

[3]Laboratório de Grupo TRACKs, Programa de Pós-graduação em Ciência dos Materiais, Universidade Federal de São Carlos – UFSCar, Sorocaba, SP, Brasil

**giovannimiraveti@estudante.ufscar.br*

Abstract

Polyurethanes, versatile polymers extensively explored across industries, can be augmented by incorporating complementary materials like lanthanides. This research presents a novel approach, employing a one-shot synthesis to create polyurethane-lanthanide composites using polyol, isocyanate, samarium, and holmium oxides. FTIR and Raman spectroscopy affirmed successful polyurethane matrix formation, while XRD unveiled distinct phases in lanthanide-loaded matrices versus soft, low-crystallinity polyurethane in control foam. Optical microscopy displayed morphology alterations due to samarium and holmium. Thermogravimetric analysis revealed heightened composite thermal stability compared to control foam. Looking ahead, these outcomes prompt further exploration of polyurethane-lanthanide composites, particularly in harnessing property changes for diverse applications.

Keywords: *composite, holmium, lanthanides, polyurethane, samarium.*

How to cite: Alves, L. R., Carriello, G. M., Pegoraro, G. M., Lopes, H. S. M., Janolla, T. A., Dias, A. N. C., Mambrini, G. P., Rezende, M. L., & Menezes, A. J. (2023). Synthesis and characterization of polyurethane and samarium(III) oxide and holmium(III) oxide composites. *Polímeros: Ciência e Tecnologia*, *33*(4), e20230039. https://doi.org/10.1590/0104-1428.20230023

1. Introduction

Modern days, along with the need for increasingly durable and practical products, have caused many traditional materials to be replaced, especially by polymers, due to their numerous applications and properties[1,2]. Among the various types of polymeric materials on the market, polyurethane (PU), developed in 1937 by Otto Bayer and collaborators, stands out in terms of its versatility and applicability[2-4].

PU is synthesized through a polymerization reaction between a chemical called polyol, which contains hydroxyl groups (-OH), and another substance containing functional isocyanate groups (-NCO), which will result in a monomer product called urethane in an exothermic reaction[4,5]. The most common process for the synthesis of PU is the so-called batch process, also called one-shot, which consists of mixing the reagents and then stirring vigorously in a one-step process, then the reagents are poured into the desired mold[6].

PU can be found in the flexible or rigid foam form, as well as thermoplastic, adhesive, coating, binder, sealant, elastomer, fiber, and resins dispersed in water[3,5,7]. Due to its wide array of conformations, this polymer is generally applied in implants, footwear[8], cars, fabrics and can present several properties, such as good thermal stability, mechanical[3,9], hydrolytic, platelet adhesion[10], shape memory[11], chemical resistance and biocompatibility[12,13].

To change PU properties, such as flame retardance, ignition, and degradation temperature, additives can be mixed in the structure[14,15]. Recent research indicates that PU structures with added lanthanides provide different properties to the final material, such as fluorescence, magnetic properties, protection against ultraviolet radiation, and flame retardancy, resulting in promising applications and indicating potentialities in research involving PU and lanthanide elements[7,16-18].

The lanthanides refer to the group of elements in the periodic table with atomic numbers 57 to 71, from lanthanum to lutetium[19]. The lanthanides are also the major constituents of the rare earth elements, which consist of the lanthanides plus yttrium and scandium[20]. These elements show similarity to physical and chemical properties, causing them to be categorized in this group[19,20]. Several studies report the use of a polymer matrix with lanthanides for different applications, such as magnetically responsive

polymer[21], fluorescence enhancement[22], nanoparticles for high resolution[23] and electrospun nanofibers[24,25].

Currently, the biggest producer of rare earth elements is China, with about 40% of the world's reserve of ores from which these elements are extracted[20,26]. Brazil, in turn, has the third largest ore reserves in the world but does not exploit them as much[26-28]. Bearing in mind the previously presented points, this article presents a study of the synthesis and characterization of PU with samarium(III) oxide and holmium(III) oxide, contributing to recent research in this area. Recently conducted systematic reviews reveal that the combination of polyurethane with samarium or holmium has not yet been explored in the literature[29].

2. Materials and Methods

2.1 Chemicals

Commercial polyol (Redelease, Brazil), commercial isocyanate (2,4'-diphenylmethane diisocyanate, Redelease, Brazil), Sm_2O_3 99,99% (Moscow 7 Store, China) and Ho_2O_3 (Sanyinghe, China).

2.2 Synthesis

The polyurethane was synthesized by the one-shot method, which consists of the synthesis through the stirred mixture of the polyol with the isocyanate for 60 seconds at 300 RPM[6,30,31] under heating at 75 °C. Due to the heating in the synthesis, pure samples were named HPU referring to no added lanthanides. To prepare the sample without lanthanide oxides, a 1:1 mass ratio of polyol to isocyanate mass was used.

For samples containing Sm_2O_3 and Ho_2O_3, mixtures containing oxide percentages of 5%, 10%, 15%, 20% and 25% were prepared, according to Equation 1, maintaining the 1:1 mass ratio of polyol to isocyanate. These were named HPU followed by the lanthanide it contained and its mass percentage.

$$\%_{lanthanide} = \frac{mass\ of\ lanthanide\ oxide}{polyol\ mass + mass\ of\ isocyanate} \quad (1)$$

In all samples, the corresponding lanthanide oxide was mixed with the heated isocyanate before reaction with the polyol. The samples were allowed to rest for one week before the characterizations.

2.3 Characterizations

2.3.1 Fourier-transform infrared spectroscopy (FTIR)

Measurements of the powder samples were performed in a Perkin Elmer Frontier (Massachusetts, USA) equipment with an Attenuated Total Reflection (ATR) apparatus, from wavenumbers of 4000 to 400 cm^{-1}, with a resolution of 4 cm^{-1} and 64 scans.

2.3.2 Raman spectroscopy

Micro-Raman Spectroscopy was performed in a Renishaw in-Via Reflex coupled to a microscope, using a diode laser of 532 nm and 500 mW. Samples were analyzed from 500 to 4000 cm^{-1} spectral range, 3 s of exposure, and 3 accumulations.

2.3.3 X-ray powder Diffraction (XRD)

A Shimadzu XRD-6100 diffractometer was used operating at a voltage of 40.0 kV and current of 30.0 mA with a copper X-ray tube. Continuous scans were performed at a speed of 2.0 °C·min^{-1} in the 2 theta range of 10º to 37º. The analyzed sample was in powder.

2.3.4 Thermogravimetric (TG)

Thermal decomposition properties were evaluated TG in a Perkin Elmer Pyris (Massachusetts, USA) equipment, from 30 ºC to 750 °C and a heating rate of 10 °C·min^{-1} under nitrogen (N_2) atmosphere of 20 mL·min^{-1}. Values for T_{max} were obtained from the maximum height of the decomposition peak for each sample. Sample masses were normalized by subtracting lanthanide mass that was already in the sample, as these metallic oxides would not degrade at the analyzed temperatures.

2.3.5 Optic microscopy

A Leica EZ4W optical microscope coupled to a microcomputer was used to obtain the images under 35x magnification.

3. Results and Discussion

3.1 Vibrational spectroscopy: FTIR and Raman

The FTIR and micro-Raman spectra of all samples are shown in Figure 1. According to Trovati et al. (2010)[32], the peak at approximately 2270 cm^{-1} corresponds to the -N=C=O groups from isocyanates. The increasing content of samarium and holmium increased this peak intensity, which may indicate that either its presence hinders the polymerization between the isocyanates and the polyols, resulting in remaining unreacted molecules[32], which may be due to an excess of isocyanate or other interactions may have occurred during the synthesis between the PU matrix and the lanthanides. This perception of increased intensity was noted by standardizing the height of the peak in the region of 1600 cm^{-1}, referring to the C=C of the aromatic ring[33], since this does not participate in the reaction.

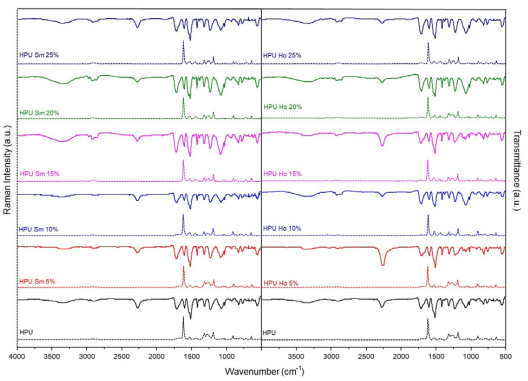

Figure 1. FTIR and micro-Raman spectra of all samples with increasing content of samarium (left) and holmium (right) from bottom to top: pure, 5%, 10%, 15%, 20%, and 25%.

The bands corresponding to hydroxyl groups at 3300 cm^{-1} regions are more evident with increased content of Sm (mainly 15, 20 and 25% w/w) and for Ho (10, 20 and 25% w/w) oxides, which may indicate a softer polymer structure, due to a decrease in the cross-linking process between the isocyanate and polyol[32].

The bands present in the 1710 cm^{-1} region are related to the carbonyl groups and they are also evident in spectrums with increased isocyanate peaks at 2270 cm^{-1}. This information endorses the presence both as an excess isocyanate of the reaction and as polyurethanes[32].

Philip et al.[24] highlight that the presence of lanthanide complexes in poly(methyl methacrylate) (PMMA) matrix blue shifted the carbonyl peak compared to the pure matrix, indicating that some interaction may be occurring with the lanthanide complexes[24]. Kohri et al.[21] observed the similar behaviour[21]. In the latter, the authors suggest that a coordination of the carbonyl groups to the lanthanide cations may have occurred.

The C-H symmetric and non-symmetric stretching appears at 2975 and 2920 cm^{-1}, being more pronounced in the samples with higher content of lanthanides, 15, 20, and 25% (w/w) for Sm and 10, 20, and 25% (w/w) for Ho, accompanied by bands nearing 1600 and 1510 cm^{-1}, typical of polymerized urethanes with stretching C=O and N-H bonds[32]. The spectrum characteristics observed here are typical of pure PU, with changes in certain bands from isocyanates and polyols, due to the presence of Sm or Ho in the composition.

Regarding micro-Raman spectra, band assignments were identify according to the literature. Normally, the vibrational properties of lanthanides oxides or ceramics are performed in different spectrum regions, as can be observed in previous works[34]. In this study, the spectrum differences related to the organic matrix of PU are analyzed in the presence of lanthanides.

Raman scattering intensities of isocyanates were observed at the 1439 cm^{-1} region[35-37], where only the HPU Sm 25% sample presented a blue shift of this band to 1445 cm^{-1}. Urethane amides were assigned to 1185, 1255, and 1615 cm^{-1}[36], and are related to the polyurethane matrix, while the 1666 cm^{-1} region corresponds to C=C stretching vibrations[37]. However, the authors mentioned that these bands could be overlapped by multiple peaks and/or low signal-to-noise ratios. Nitrogen-containing bonds (C-N and N-H) were observed at 1527 cm^{-1}[35-37] and at 1710 cm^{-1}, while some residual carbonyl was observed and may be related to the synthesis itself[35-37]. Blue shifts in the carbonyl band were observed with increasing Sm content and may indicate some polymerization interaction between the components. The increasing content of lanthanide resulted in the appearance of a band at 2935 cm^{-1} region, more evident in samples of Sm 10% to 25% and Ho 20% and 25%, being related to C-H bonds.

3.2 X-ray diffractometry

Figure 2 shows the diffractograms of the pure polyurethane sample and samples containing Sm_2O_3 (samples Sm 5% to 25%). A characteristic band of pure polyurethane is observed around 19º, although it is wide in relation to other previous studies, indicating low crystallinity[32,33,38]. Furthermore, the absence of bands at 11° shows that the polyurethane is of the soft type, given that the polyol hydroxyl groups change the product's crosslinking[32].

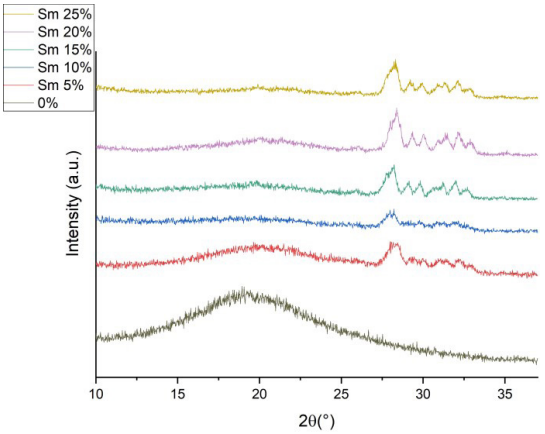

Figure 2. X-ray diffractograms of samples containing 5%, 10%, 15%, 20%, and 25% Sm_2O_3.

The samples containing Sm_2O_3 showed peaks at 28,3°, 29,3°, 29,9°, 31,3°, 32,1°, and 32,9°, which are characteristic of monoclinic Sm_2O_3, according to the JCPDS 84-1878 sheet[39-41]. Furthermore, such peaks show that the material is a composite, since the Sm_2O_3 remained crystalline, forming a multiphase material with the polyurethane or different components on a microscopic scale. This characteristic is consistent with other works involving composites of metal oxides with polyurethane[42-44].

In the work of Deng et al.[43], pure polyurethane also showed an enlarged band around 19º, which was no longer identified with the addition of only a 2% mass ratio of ZrO_2, a relative amount much lower than the present work[44]. Other authors also attribute the decrease in the characteristic peak of polyurethane to the excessive addition of the oxide, in that case, TiO_2, which leads to the formation of additional phase aggregates and ends up reducing the crystallinity, again with only a 2% mass ratio[43].

Figure 3 shows the diffractograms of the pure polyurethane sample and samples containing Ho_2O_3 (samples Ho 5% to 25%). The behavior observed in the Ho samples is similar to that of samples containing Sm_2O_3 (Figure 2). In this way, it is possible to state that it is a soft polyurethane composite with Ho_2O_3. The peaks in the diffractogram at 20,6°, 29,2°, 33,9° and 35,9° are characteristic of cubic Ho_2O_3, in accordance with the JCPDS 83-0932 sheet[45,46].

The results for the addition of Ho_2O_3 in the polymeric matrix are also comparable to those previously obtained and discussed in the literature. Larger relative masses, such as 30% of Fe_2O_3, also indicated peaks corresponding only to the oxide, while the pure polyurethane showed only the broad band at 19º[42].

3.3 Thermogravimetry (TG)

The TG and DTG curves of all samples with samarium are shown in figures 4 and 5. Table 1 contains T_{max} and mass values for the decomposition peaks presented by samples.

According to the literature[32], PU presents three major thermal events atributted of decomposition reaction. First,

Table 1. Values of T_{max} for each sample with samarium obtained by the decomposition steps and the approximate mass loss.

Sample	1st step (°C)	Mass loss* (%)	2nd step (°C)	Mass loss* (%)	3rd step (°C)	Remaining mass** (%)
HPU	240.31	6.64	365.46	40.89	474.07	17.78
HPU Sm 5%	250.95	2.84	348.68	28.12	473.60	14.10
HPU Sm 10%	261.79	3.32	348.61	25.91	493.57	16.98
HPU Sm 15%	252.91	6.89	342.93	32.28	474.46	18.26
HPU Sm 20%	241.34	3.86	359.32	29.24	481.67	19.42
HPU Sm 25%	252.39	5.87	346.83	32.81	490.61	9.93

*Mass loss up to this point. **Obtained from the last point of TG curve.

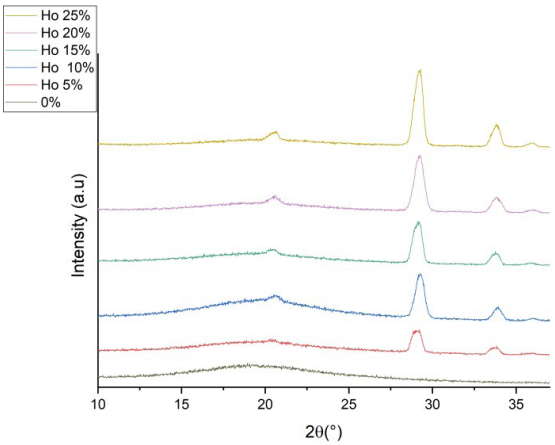

Figure 3. X-ray diffractograms of samples containing 5%, 10%, 15%, 20%, and 25% Ho_2O_3.

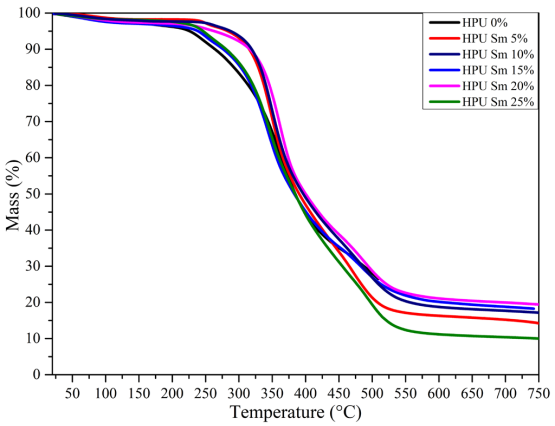

Figure 4. TG curves of all samples with samarium.

the break of urethane bonds and second thermal event, which can be separated into two steps, the ester decomposition, the latter being separated into two steps, also observed by others in a similar composite[47]. The authors state that the first step occurs, approximately, from 200 to 350°C, and the second and third range from 350 to 535°C, similar to that which was observed in figure 5. These observations suggest that all thermal decompositions observed are related to the PU matrix[32].

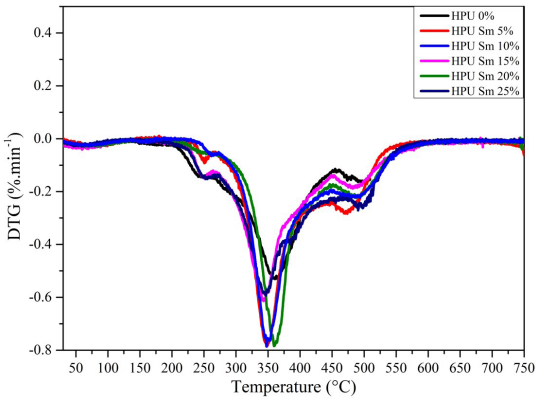

Figure 5. DTG curves of all samples with samarium.

It is possible to observe that the increased content of Sm produced greater thermal stability through decreased mass loss and higher T_{max} between 200 and 350 °C, being related to the break of urethane bonds, except for HPU Sm 15%. This suggests that the presence of lanthanide hinders the decomposition of this type of bonding. Alterations in FTIR bands can be observed above, where the addition of lanthanides modified isocyanate and carbonyl regions, also observed in the literature[21,23,24] and highlighted by Wang et al.[47]. Further investigations should be performed to better understand these.

Only HPU Sm 20% maintained the lowest mass loss rate during the entire analysis, presenting the greater remaining mass of 19.42%, with the highest T_{max} value for the second decomposition peak amongst all samples with Sm, which may be related to the highest alteration on the carbonyl and isocyanate bands, as observed in FTIR results. However, all samples with Sm presented a lower T_{max} value for this peak, compared to pure HPU. As expected, the greater percentage of Sm in the sample composition increased the remaining mass, except for HPU Sm 25%, presenting the lowest remaining mass of all samples, which may indicate that this amount of Sm did not play an important role in the HPU decomposition, since its FTIR spectrum presented lower alterations.

Additionally, the TG and DTG curves of all samples with holmium are shown in Figures 6 and 7. Table 2 also contains T_{max} and mass values for the decomposition peaks presented by samples.

The same observation made for the samples with samarium is replicated in the samples with holmium, i.e., presenting three major steps of decomposition[32,47].

Table 2. Values of T_{max} for each sample with holmium obtained by the decomposition steps and the approximate mass loss.

Sample	1st step (°C)	Mass loss* (%)	2nd step (°C)	Mass loss* (%)	3rd step (°C)	Remaining mass** (%)
HPU	240.31	6.64	365.46	40.89	474.07	17.78
HPU Ho 5%	259.92	4.87	359.47	30.12	498.39	21.69
HPU Ho 10%	243.73	8.58	391.06	55.4	460.71	3.89
HPU Ho 15%	246.00	3.50	348.21	31.48	431.84	9.62
HPU Ho 20%	246.79	3.55	354.76	28.43	493.62	17.97
HPU Ho 25%	247.94	6.54	359.52	36.40	497.53	21.07

*Mass loss up to this point. **Obtained from the last point of TG curve.

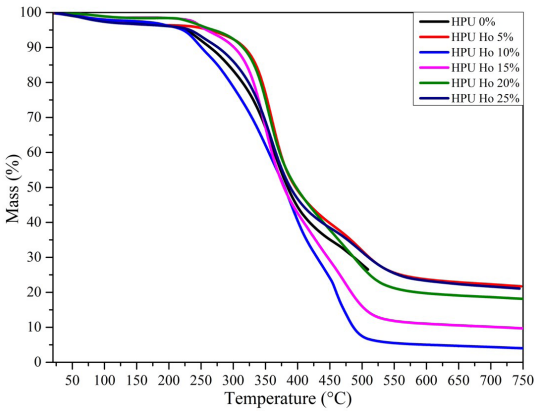

Figure 6. TG curves of all samples with holmium.

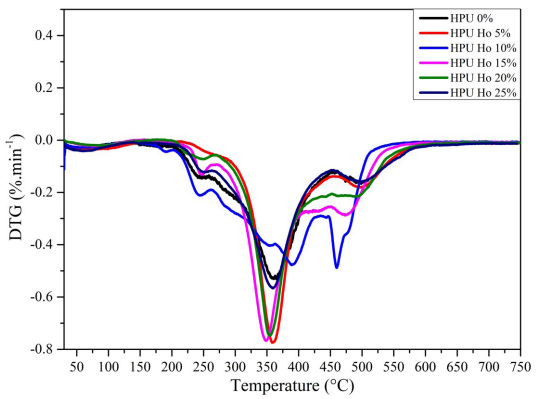

Figure 7. DTG curves of all samples with holmium.

The presence of holmium also promoted higher thermal stability on the samples, observed through the decreased mass loss presented after the decomposition steps occurred, except for the sample HPU Ho 10%, which showed a particular behavior, presenting higher and non-linear mass loss in the first and second steps of decomposition and lower remaining mass. This sample had the highest alteration in the FTIR spectrum, with increased intensities for hydroxyl groups, C-H, and carbonyl bands, indicating some interactions may have occurred, modifying the decomposition kinetics[21,24,47].

Can be observed that all samples presented a decreased T_{max} value for the second decomposition peak, indicating that the presence of lanthanide should have promoted an intensified ester decomposition[32]. Samples HPU Ho 5%, and 25% presented higher thermal stability during the entire analysis, with the highest T_{max} and remaining mass values for all decomposition peaks, similar to that observed for HPU Sm 20%. In general, samples with the greater amount of holmium did not present a linear behavior of remaining mass, which may indicate a formation of complexes that promote higher or lower decomposition of the HPU matrix, which should be systematically investigated, already mentioned by others[47].

Philip et al.[24] observed some alterations in carbonyl bands with the addition of lanthanide complexes in the PMMA matrix, confirming through several microscopy techniques the presence of lanthanide complexes within the PMMA matrix due to its porous surface, which may have also occurred here to HPU[24]. Nevertheless, higher alterations in hydroxyl, isocyanate, and carbonyl bands may have played a role in this observation[21,24].

The presence of both lanthanides increased the thermal stability of urethane bonds of HPU, observed through higher T_{max} and lower mass loss values for the first decomposition peak. Regarding the ester decomposition second peak, the presence of both lanthanides intensified its decomposition, through lower T_{max} observed, but maintained some thermal stability through lower mass loss.

3.4 Optic microscopy

In Figure 8b, it can be noticed that the HPU cells containing 5% Ho present a certain regularity in size with an elliptical shape. However, when the amount of holmium is increased, cells begin to lose this regularity, as in Figure 8c, d, e, and f, thus showing the appearance of tears within their morphology, as well as demonstrating smaller cell dimensions[48].

The decrease in the size of the polymer cell is observed with the increase of the holmium mass amount, which may indicate an increase in cell crosslinking and which may end up affecting the cell nucleation process[49].

By cross-sectional view analysis of the control foam we can be seen that it had the largest cell dimension when compared to the foams containing Ho and Sm, shown in Figure 9. This phenomenon can be explained by the reaction of isocyanate with the polyol, in which one of its products is carbon dioxide (CO_2), which demonstrates that the addition of lanthanides ends up proportionally decreasing the size of the foam cells, which may end up diffusing within the

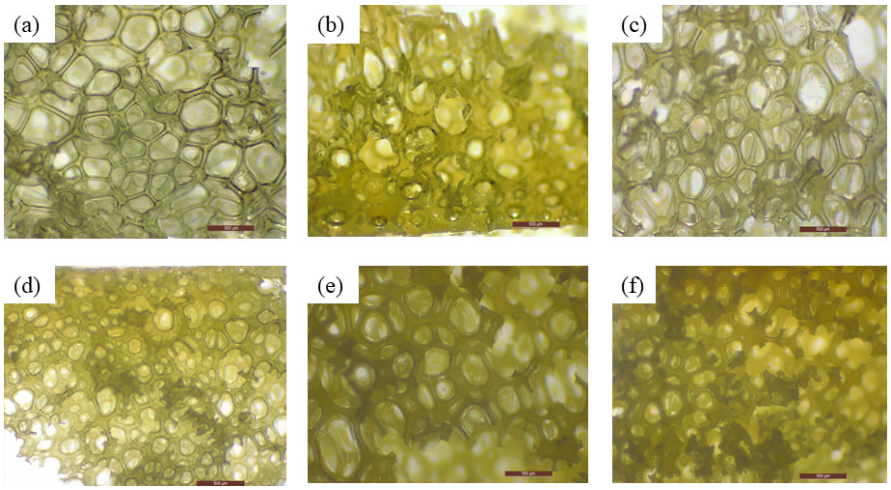

Figure 8. Morphology of the cross-section structure of HPU foams with 35x magnification containing holmium: (a) Control or HPU; (b) Ho 5%; (c) Ho 10%; (d) Ho 15%; (e) Ho 20%, and (f) Ho 25%.

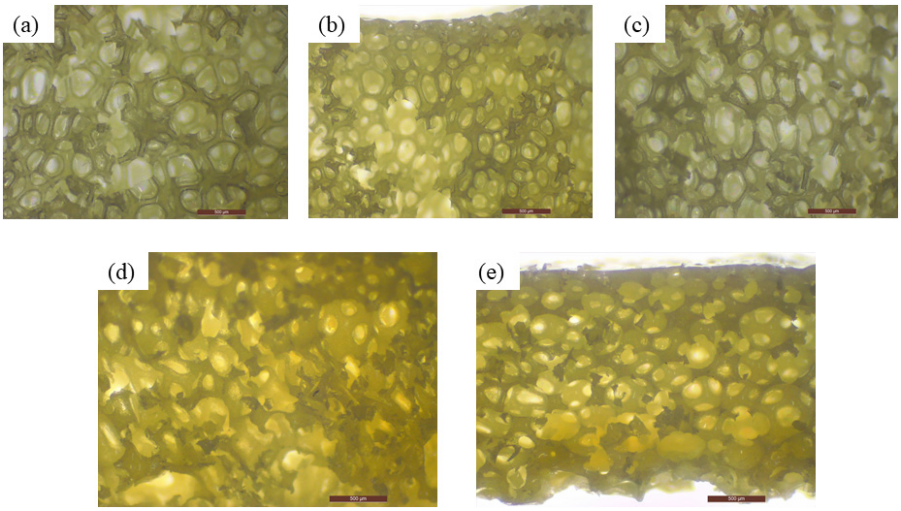

Figure 9. Morphology of the cross-section structure of HPU foams with 35x magnification containing samarium: (a) Sm 5%; (b) Sm 10%; (c) Sm 15%; (d) Sm 20%, and (e) Sm 25%.

lanthanide structure since the control foam had the largest pores of all foams[2,50].

Analyzing the morphologies of structures containing HPU with samarium in the cross-sectional view, it can be seen that cells containing 5% Sm mass, Figure 9a, are larger than those containing 5% Ho, Figure 8b. Thus, the addition of a samarium can significantly influence cell size and shape[51,52].

In addition, due to the morphological structure presenting itself as a polygon shape, this may indicate a lower stability due to its interface area, since the greater the cell interface area, the greater its surface energy[53]. The increase in the amount of samarium relative mass caused the cells to decrease in size due to the interfacial adhesion of the inorganic load as demonstrated in Figures 9b, c, d, and e, which may indicate that samarium has a hydrophobic surface nature, which when in contact with the hydrophilic matrix of the HPU ends up causing a collapse between cells. This phenomenon is even more noticeable when increasing the amount of samarium inside the matrix[54].

4. Conclusions

Through the FTIR technique, it was possible to observe that successfully obtained polyurethane foams containing holmium oxide and samarium oxide, by means of the vibrational spectra of urethane bond formation. The addition of lanthanide oxides caused shifts in the main FTIR and Raman bands, which may indicate a potential interaction with the reagents used, such as polyol and isocyanate.

The XRD technique demonstrated the presence of two distinct phases: one related to the low crystallinity of the polyurethane and the other due to the crystallinity of the lanthanide oxides. The morphology analyzed

through the optical microscope showed that the addition of lanthanides proportionally altered the shape and size of the cells. Thermogravimetric analyses demonstrated that the incorporation of holmium and samarium improved the thermal properties of the material, which, with further investigation, could be used as flame retardants.

5. Author's Contribution

• **Conceptualization** – Lucas Repecka Alves; Giovanni Miraveti Carriello; Guilherme Manassés Pegoraro.

• **Data curation** – Giovanni Miraveti Carriello; Henrique Solowej Medeiros Lopes; Thaís de Agrella Janolla.

• **Formal analysis** – Lucas Repecka Alves; Giovanni Miraveti Carriello; Guilherme Manassés Pegoraro; Henrique Solowej Medeiros Lopes; Thaís de Agrella Janolla.

• **Funding acquisition** - NA.

• **Investigation** – Aparecido Junior de Menezes; Maira de Lourdes Rezende; Giovanni Pimenta Mambrini; Airton Natanael Coelho Dias.

• **Methodology** – Lucas Repecka Alves; Giovanni Miraveti Carriello.

• **Project administration** – Aparecido Junior de Menezes; Maira de Lourdes Rezende; Giovanni Pimenta Mambrini; Airton Natanael Coelho Dias.

• **Resources** – Aparecido Junior de Menezes; Maira de Lourdes Rezende; Giovanni Pimenta Mambrini; Airton Natanael Coelho Dias.

• **Software** – NA.

• **Supervision** – Aparecido Junior de Menezes; Maira de Lourdes Rezende; Giovanni Pimenta Mambrini; Airton Natanael Coelho Dias.

• **Validation** – Aparecido Junior de Menezes; Maira de Lourdes Rezende; Giovanni Pimenta Mambrini; Airton Natanael Coelho Dias.

• **Visualization** – Aparecido Junior de Menezes; Maira de Lourdes Rezende; Giovanni Pimenta Mambrini; Airton Natanael Coelho Dias.

• **Writing – original draft** – Lucas Repecka Alves; Giovanni Miraveti Carriello; Guilherme Manassés Pegoraro; Henrique Solowej Medeiros Lopes; Thaís de Agrella Janolla.

• **Writing – review & editing** – Aparecido Junior de Menezes; Maira de Lourdes Rezende; Giovanni Pimenta Mambrini; Airton Natanael Coelho Dias.

6. Acknowledgements

This study was financed in part by the Coordenação de Aperfeiçoamento de Pessoal de Nível Superior – Brasil (CAPES) – Finance Code 001.

7. References

1. Aquino, F. G., Sheldrake, T., Clevelario, J., Pires, F., & Coutinho, F. M. B. (2010). Estudo do envelhecimento de poliuretanos aplicados na indústria de petróleo. *Polímeros: Ciência e Tecnologia*, *20*(1), 33-38. http://dx.doi.org/10.1590/S0104-14282010005000006.
2. Alves, L. R., Carriello, G. M., Pegoraro, G. M., & Fernandes, J., Fo. (2021). A utilização de óleos vegetais como fonte de polióis para a síntese de poliuretano: uma revisão. *Disciplinarum Scientia. Série Naturais e Tecnológicas*, *22*(1), 99-118. http://dx.doi.org/10.37779/nt.v22i1.3711.
3. Akindoyo, J. O., Beg, M. D. H., Ghazali, S., Islam, M. R., Jeyaratnam, N., & Yuvaraj, A. R. (2016). Polyurethane types, synthesis and applications: a review. *RSC Advances*, *6*(115), 114453-114482. http://dx.doi.org/10.1039/C6RA14525F.
4. Coutinho, F. M. B., & Delpech, M. C. (1999). Poliuretanos como materiais de revestimento de superfície. *Polímeros: Ciência e Tecnologia*, *9*(1), 41-48. http://dx.doi.org/10.1590/S0104-14281999000100006.
5. Gama, N. V., Ferreira, A., & Barros-Timmons, A. (2018). Polyurethane foams: past, present, and future. *Materials*, *11*(10), 1841. http://dx.doi.org/10.3390/ma11101841. PMid:30262722.
6. Macedo, V., Zimmermmann, M. V. G., Koester, L. S., Scienza, L. C., & Zattera, A. J. (2017). Obtenção de espumas flexíveis de poliuretano com celulose de *Pinus elliottii. Polímeros: Ciência e Tecnologia*, *27*(5), 27-34. http://dx.doi.org/10.1590/0104-1428.2212.
7. Ma, G., Guan, T., Hou, C., Wu, J., Wang, G., Ji, X., & Wang, B. (2015). Preparation, properties and application of waterborne hydroxyl-functional polyurethane/acrylic emulsions in two-component coatings. *Journal of Coatings Technology and Research*, *12*(3), 505-512. http://dx.doi.org/10.1007/s11998-014-9647-y.
8. Davis, F. J., & Mitchell, G. R. (2008). *Polyurethane based materials with applications in medical devices.* In P. Bártolo & B. Bidanda (Eds.), *Bio-materials and prototyping applications in medicine* (pp. 27-48). Boston: Springer. http://dx.doi.org/10.1007/978-0-387-47683-4_3.
9. Llevot, A., & Meier, M. (2019). Perspective: green polyurethane synthesis for coating applications. *Polymer International*, *68*(5), 826-831. http://dx.doi.org/10.1002/pi.5655.
10. Król, P. (2007). Synthesis methods, chemical structures and phase structures of linear polyurethanes. Properties and applications of linear polyurethanes in polyurethane elastomers, copolymers and ionomers. *Progress in Materials Science*, *52*(6), 915-1015. http://dx.doi.org/10.1016/j.pmatsci.2006.11.001.
11. Kausar, A. (2020). Shape memory polyurethane/graphene nanocomposites: structures, properties, and applications. *Journal of Plastic Film & Sheeting*, *36*(2), 151-166. http://dx.doi.org/10.1177/8756087919865296.
12. Bahrami, S., Solouk, A., Mirzadeh, H., & Seifalian, A. M. (2019). Electroconductive polyurethane/graphene nanocomposite for biomedical applications. *Composites. Part B, Engineering*, *168*, 421-431. http://dx.doi.org/10.1016/j.compositesb.2019.03.044.
13. Cong, L., Yang, F., Guo, G., Ren, M., Shi, J., & Tan, L. (2019). The use of polyurethane for asphalt pavement engineering applications: a state-of-the-art review. *Construction & Building Materials*, *225*, 1012-1025. http://dx.doi.org/10.1016/j.conbuildmat.2019.07.213.
14. Singh, H., & Jain, A. K. (2009). Ignition, combustion, toxicity, and fire retardancy of polyurethane foams: a comprehensive review. *Journal of Applied Polymer Science*, *111*(2), 1115-1143. http://dx.doi.org/10.1002/app.29131.
15. Vahabi, H., Rastin, H., Movahedifar, E., Antoun, K., Brosse, N., & Saeb, M. R. (2020). Flame retardancy of bio-based polyurethanes: opportunities and challenges. *Polymers*, *12*(6), 1234. http://dx.doi.org/10.3390/polym12061234. PMid:32485825.
16. Wang, X., Zhou, S., & Wu, L. (2012). Stability, UV shielding properties, and light conversion behavior of Eu(BMDM)3@ polysiloxane nanoparticles in water and polyurethane films.

Materials Chemistry and Physics, *137*(2), 644-651. http://dx.doi.org/10.1016/j.matchemphys.2012.09.070.

17. Villagra, D., Fuentealba, P., Spodine, E., Vega, A., Santana, R. C., Verdejo, R., Lopez-Manchado, M. A., & Aguilar-Bolados, H. (2021). Effect of terbium(III) species on the structure and physical properties of polyurethane (TPU). *Polymer*, *233*, 124209. http://dx.doi.org/10.1016/j.polymer.2021.124209.
18. Yin, Z., Lu, J., Yu, X., Jia, P., Tang, G., Zhou, X., Lu, T., Guo, L., Wang, B., Song, L., & Hu, Y. (2021). Construction of a core-shell structure compound: ammonium polyphosphate wrapped by rare earth compound to achieve superior smoke and toxic gases suppression for flame retardant flexible polyurethane foam composites. *Composites Communications*, *28*, 100939. http://dx.doi.org/10.1016/j.coco.2021.100939.
19. Farnaby, J. H., Chowdhury, T., Horsewill, S. J., Wilson, B., & Jaroschik, F. (2021). Lanthanides and actinides: annual survey of their organometallic chemistry covering the year 2019. *Coordination Chemistry Reviews*, *437*, 213830. http://dx.doi.org/10.1016/j.ccr.2021.213830.
20. Ganguli, R., & Cook, D. R. (2018). Rare earths: a review of the landscape. *MRS Energy & Sustainability*, *5*(1), 6. http://dx.doi.org/10.1557/mre.2018.7.
21. Kohri, M., Yanagimoto, K., Kohaku, K., Shiomoto, S., Kobayashi, M., Imai, A., Shiba, F., Taniguchi, T., & Kishikawa, K. (2018). Magnetically responsive polymer network constructed by poly(acrylic acid) and holmium. *Macromolecules*, *51*(17), 6740-6745. http://dx.doi.org/10.1021/acs.macromol.8b01550.
22. Jiu, H., Zhang, L., Liu, G., & Fan, T. (2009). Fluorescence enhancement of samarium complex co-doped with terbium complex in a poly(methyl methacrylate) matrix. *Journal of Luminescence*, *129*(3), 317-319. http://dx.doi.org/10.1016/j.jlumin.2008.10.015.
23. Cao, F., Huang, T., Wang, Y., Liu, F., Chen, L., Ling, J., & Sun, J. (2015). Novel lanthanide-polymer complexes for dye-free dual modal probes for MRI and fluorescence imaging. *Polymer Chemistry*, *6*(46), 7949-7957. http://dx.doi.org/10.1039/C5PY01011J.
24. Philip, P., Thomas, P., Jose, E. T., Philip, K. C., & Thomas, P. C. (2019). Structural and optical properties of synthesized poly(methyl methacrylate) (PMMA) and lanthanide β-diketonate complexes incorporated electrospun PMMA nanofibres for optical devices. *Bulletin of Materials Science*, *42*(5), 218. http://dx.doi.org/10.1007/s12034-019-1893-2.
25. Philip, P., Jose, T., Jose, A., & Cherian, S. K. (2021). Studies on the structural and optical properties of samarium β-diketonate complex incorporated electrospun poly(methylmethacrylate) nanofibres with different architectures. *Luminescence*, *36*(4), 1032-1047. http://dx.doi.org/10.1002/bio.4029. PMid:33570221.
26. Dang, D. H., Thompson, K. A., Ma, L., Nguyen, H. Q., Luu, S. T., Duong, M. T. N., & Kernaghan, A. (2021). Toward the circular economy of rare earth elements: a review of abundance, extraction, applications, and environmental impacts. *Archives of Environmental Contamination and Toxicology*, *81*(4), 521-530. http://dx.doi.org/10.1007/s00244-021-00867-7. PMid:34170356.
27. Serra, O. A. (2011). Rare earths: Brazil × China. *Journal of the Brazilian Chemical Society*, *22*(5), 811-812. http://dx.doi.org/10.1590/S0103-50532011000500001.
28. Sousa, P. C., Fo., & Serra, O. A. (2014). Rare earths in Brazil: historical aspects, production, and perspectives. *Quimica Nova*, *37*(4). http://dx.doi.org/10.5935/0100-4042.20140121.
29. Pegoraro, G. M., Alves, L. R., Carriello, G. M., Janolla, T. A., Mambrini, G. P., Rezende, M. L., & Menezes, A. J. (2023). Polyurethane and rare-earth materials: a review. *The Journal of Engineering and Exact Sciences*, *9*(3), 15627-01e. http://dx.doi.org/10.18540/jcecvl9iss3pp15627-01e.
30. Prisacariu, C., Scortanu, E., & Agapie, B. (2011). Synthesis and characterization of dibenzyl based polyurethane blends obtained via the one shot synthesis route. *Procedia Engineering*, *10*, 984-989. http://dx.doi.org/10.1016/j.proeng.2011.04.162.
31. Cinelli, P., Anguillesi, I., & Lazzeri, A. (2013). Green synthesis of flexible polyurethane foams from liquefied lignin. *European Polymer Journal*, *49*(6), 1174-1184. http://dx.doi.org/10.1016/j.eurpolymj.2013.04.005.
32. Trovati, G., Sanches, E. A., Claro Neto, S., Mascarenhas, Y. P., & Chierice, G. O. (2010). Characterization of polyurethane resins by FTIR, TGA, and XRD. *Journal of Applied Polymer Science*, *115*(1), 263-268. http://dx.doi.org/10.1002/app.31096.
33. Gao, X., Zhu, Y., Zhao, X., Wang, Z., An, D., Ma, Y., Guan, S., Du, Y., & Zhou, B. (2011). Synthesis and characterization of polyurethane/SiO_2 nanocomposites. *Applied Surface Science*, *257*(10), 4719-4724. http://dx.doi.org/10.1016/j.apsusc.2010.12.138.
34. Dias, A., Khalam, L. A., Sebastian, M. T., Lage, M. M., Matinaga, F. M., & Moreira, R. L. (2008). Raman scattering and infrared spectroscopy of chemically substituted Sr_2LnTaO_6 (Ln = Lanthanides, Y, and In) Double Perovskites. *Chemistry of Materials*, *20*(16), 5253-5259. http://dx.doi.org/10.1021/cm800969m.
35. Romanova, V., Begishev, V., Karmanov, V., Kondyurin, A., & Maitz, M. F. (2002). Fourier transform Raman and Fourier transform infrared spectra of cross-linked polyurethaneurea films synthesized from solutions. *Journal of Raman Spectroscopy: JRS*, *33*(10), 769-777. http://dx.doi.org/10.1002/jrs.914.
36. Parnell, S., Min, K., & Cakmak, M. (2003). Kinetic studies of polyurethane polymerization with Raman spectroscopy. *Polymer*, *44*(18), 5137-5144. http://dx.doi.org/10.1016/S0032-3861(03)00468-3.
37. Socrates, G. (2001). I*nfrared and Raman characteristic group frequencies: tables and charts*. Chichester: John Wiley & Sons.
38. Alaa, M., Yusoh, K., & Hasany, S. F. (2015). Pure polyurethane and castor oil based polyurethane: synthesis and characterization. *Journal of Mechanical Engineering Science*, *8*, 1507-1515. http://dx.doi.org/10.15282/jmes.8.2015.25.0147.
39. Madhuri, S. N., & Rukmani, K. (2019). Synthesis and concentration dependent tuning of PVA-Sm_2O_3 nanocomposite films for optoelectronic applications. *Materials Research Express*, *6*(7), 075017. http://dx.doi.org/10.1088/2053-1591/ab1326.
40. Liu, T., Zhang, Shao, & Li, (2003). Synthesis and characteristics of Sm_2O_3 and Nd_2O_3 nanoparticles. *Langmuir*, *19*(18), 7569-7572. http://dx.doi.org/10.1021/la034350l.
41. Guo, Q., Zhao, Y., Jiang, C., Mao, W. L., & Wang, Z. (2008). Phase transformation in Sm_2O_3 at high pressure: in situ synchrotron X-ray diffraction study and ab initio DFT calculation. *Solid State Communications*, *145*(5-6), 250-254. http://dx.doi.org/10.1016/j.ssc.2007.11.019.
42. Park, C.-H., Kang, S.-J., Tijing, L. D., Pant, H. R., & Kim, C. S. (2013). Inductive heating of electrospun Fe_2O_3/polyurethane composite mat under high-frequency magnetic field. *Ceramics International*, *39*(8), 9785-9790. http://dx.doi.org/10.1016/j.ceramint.2013.05.042.
43. Deng, F., Zhang, Y., Li, X., Liu, Y., Shi, Z., & Wang, Y. (2019). Synthesis and mechanical properties of dopamine modified titanium dioxide/waterborne polyurethane composites. *Polymer Composites*, *40*(1), 328-336. http://dx.doi.org/10.1002/pc.24654.
44. Jothi, K. J., Balachandran, S., Mohanraj, K., Prakash, N., Subhasri, A., Krishnan, P. S. G., & Palanivelu, K. (2022). Fabrications of hybrid Polyurethane-Pd doped ZrO_2 smart carriers for self-healing high corrosion protective coatings. *Environmental Research*, *211*, 113095. http://dx.doi.org/10.1016/j.envres.2022.113095. PMid:35283074.

45. Mortazavi-Derazkola, S., Zinatloo-Ajabshir, S., & Salavati-Niasari, M. (2017). Facile hydrothermal and novel preparation of nanostructured Ho_2O_3 for photodegradation of eriochrome black T dye as water pollutant. *Advanced Powder Technology*, *28*(3), 747-754. http://dx.doi.org/10.1016/j.apt.2016.11.022.
46. Abu-Zied, B. M., & Asiri, A. M. (2019). Genesis of nanocrystalline Ho_2O_3 via thermal decomposition of holmium acetate: structure evolution and electrical conductivity properties. *Journal of Rare Earths*, *37*(2), 185-192. http://dx.doi.org/10.1016/j.jre.2018.05.017.
47. Wang, J. L., Li, Y., Chain, W., Wang, X., Li, H. T., Liu, S. H., Zhang, J. R., & Xu, M. X. (2013). Synthesis and characterization of rare earth/polyurethane composite material. *Advanced Materials Research*, *763*, 125-129. http://dx.doi.org/10.4028/www.scientific.net/AMR.763.125.
48. Carriço, C. S. (2017). *Obtenção de espumas de poliuretano a partir de coprodutos da cadeia dos biocombustíveis e resíduos agroindustriais* (Doctoral thesis). Universidade Federal de Minas Gerais, Belo Horizonte. Retrieved in 2023, March 22, from https://repositorio.ufmg.br/handle/1843/SFSA-ARZULR
49. Dolomanova, V., Rauhe, J. C. M., Jensen, L. R., Pyrz, R., & Timmons, A. B. (2011). Mechanical properties and morphology of nano-reinforced rigid PU foam. *Journal of Cellular Plastics*, *47*(1), 81-93. http://dx.doi.org/10.1177/0021955X10392200.
50. Reignier, J., Alcouffe, P., Méchin, F., & Fenouillot, F. (2019). The morphology of rigid polyurethane foam matrix and its evolution with time during foaming – New insight by cryogenic scanning electron microscopy. *Journal of Colloid and Interface Science*, *552*, 153-165. http://dx.doi.org/10.1016/j.jcis.2019.05.032. PMid:31125826.
51. Mello, D., Pezzin, S. H., & Amico, S. C. (2009). The effect of post-consumer PET particles on the performance of flexible polyurethane foams. *Polymer Testing*, *28*(7), 702-708. http://dx.doi.org/10.1016/j.polymertesting.2009.05.014.
52. Silva, R. P. (2017). *Utilização de pó de poli(tereftalato de etileno) pós-consumo e do óleo de mamona (Ricinus communis) no desenvolvimento de espuma flexível* (Master's dissertation). Universidade Federal de Campina Grande, Campina Grande. Retrieved in 2023, March 22, from http://dspace.sti.ufcg.edu.br:8080/jspui/handle/riufcg/13952
53. Santin, C. K., & Petró, F. (2022). Desenvolvimento e caracterização de espuma poliuretânica à base de Difenilmetano diisocianato (MDI) e óleo de linhaça (*Linum usitatissimun* L.). *Revista Liberato*, *23*(39), 77-88. Retrieved in 2023, March 22, from https://revista.liberato.com.br/index.php/revista/article/view/77-88
54. Sung, G., & Kim, J. H. (2017). Influence of filler surface characteristics on morphological, physical, acoustic properties of polyurethane composite foams filled with inorganic fillers. *Composites Science and Technology*, *146*, 147-154. http://dx.doi.org/10.1016/j.compscitech.2017.04.029.

Received: Mar. 22, 2023
Revised: Aug. 24, 2023
Accepted: Oct. 10, 2023